

Precision microbiome reconstitution restores bile acid mediated resistance to *Clostridium difficile*

Charlie G. Buffie^{1,2}, Vanni Bucci^{3,4}, Richard R. Stein³, Peter T. McKenney^{1,2}, Lilan Ling², Asia Gobourne², Daniel No², Hui Liu⁵, Melissa Kinnebrew^{1,2}, Agnes Viale⁶, Eric Littmann², Marcel R. M. van den Brink^{7,8}, Robert R. Jenq⁷, Ying Taur^{1,2}, Chris Sander³, Justin R. Cross⁵, Nora C. Toussaint^{2,3}, Joao B. Xavier^{2,3} & Eric G. Pamer^{1,2,8}

The gastrointestinal tracts of mammals are colonized by hundreds of microbial species that contribute to health, including colonization resistance against intestinal pathogens¹. Many antibiotics destroy intestinal microbial communities and increase susceptibility to intestinal pathogens². Among these, *Clostridium difficile*, a major cause of antibiotic-induced diarrhoea, greatly increases morbidity and mortality in hospitalized patients³. Which intestinal bacteria provide resistance to *C. difficile* infection and their *in vivo* inhibitory mechanisms remain unclear. Here we correlate loss of specific bacterial taxa with development of infection, by treating mice with different antibiotics that result in distinct microbiota changes and lead to varied susceptibility to *C. difficile*. Mathematical modelling augmented by analyses of the microbiota of hospitalized patients identifies resistance-associated bacteria common to mice and humans. Using these platforms, we determine that *Clostridium scindens*, a bile acid 7α-dehydroxylating intestinal bacterium, is associated with resistance to *C. difficile* infection and, upon administration, enhances resistance to infection in a secondary bile acid dependent fashion. Using a workflow involving mouse models, clinical studies, metagenomic analyses, and mathematical modelling, we identify a probiotic candidate that corrects a clinically relevant microbiome deficiency. These findings have implications for the rational design of targeted antimicrobials as well as microbiome-based diagnostics and therapeutics for individuals at risk of *C. difficile* infection.

Infection with *C. difficile* is a growing public health threat³. Susceptibility to infection is associated with antibiotic use³, and faecal microbiota transplant, which restores microbiota complexity, can resolve recurrent infections⁴. However, the microbiome-encoded genes and biosynthetic gene clusters⁵ critical for infection resistance remain largely undefined, limiting mechanistic understanding and development of microbiota-based therapies. We sought to identify, interrogate, and validate sources of microbiome-mediated *C. difficile* resistance. We first investigated the impact of antibiotics with diverse antimicrobial spectra on the intestinal microbiota and *C. difficile* susceptibility (Extended Data Fig. 1a). Consistent with prior work from our group², administration of clindamycin resulted in long-lasting susceptibility to infection (Fig. 1a). In contrast, ampicillin induced transient susceptibility (Fig. 1c), whereas enrofloxacin did not increase susceptibility to *C. difficile* infection (Fig. 1e). *C. difficile* toxin expression correlated significantly with *C. difficile* abundance in the intestine (Extended Data Fig. 1b). The antibiotic regimens did not substantially alter bacterial density (Extended Data Fig. 1c), but 16S ribosomal RNA (rRNA) gene amplicon sequencing revealed that the three antibiotics had distinct impacts on intestinal microbiota composition (Fig. 1b, d, f).

We exploited this variance in intestinal bacterial composition and infection susceptibility to relate features of microbiota structure to *C. difficile* inhibition. Infection susceptibility correlated with decreased

microbiota alpha diversity (that is, diversity within individuals) (Fig. 2a), consistent with previous studies⁶. Using weighted UniFrac⁷ distances to evaluate beta diversity (that is, diversity between individuals), we found that although clindamycin and ampicillin administration induced distinct changes in microbiota structure, recovery of resistance corresponded with return to a common coordinate space shared by antibiotic-naïve animals (Fig. 2b). However, these diversity metrics generally did not resolve the susceptibility status of animals harbouring microbiota with

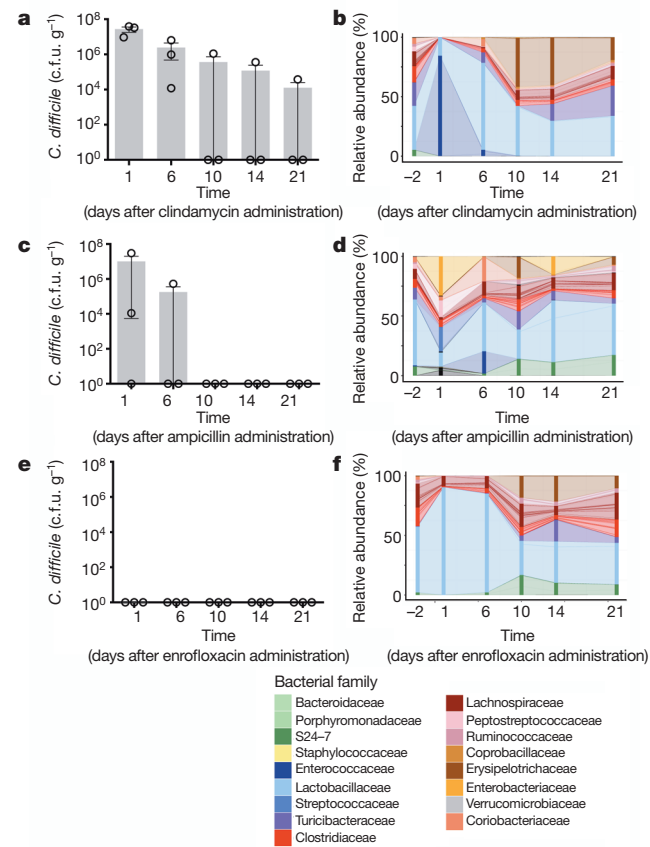


Figure 1 | Different antibiotics induce distinct changes to *C. difficile* infection resistance and intestinal microbiota composition. Susceptibility to *C. difficile* infection after administration of clindamycin (a), ampicillin (c), or enrofloxacin (e). b, d, f, Intestinal microbiota composition at time points indicated. Each stacked bar represents the mean microbiota composition of three separately housed animals. Centre values (mean), error bars (s.e.m.) (a, c, e).

¹Infectious Diseases Service, Department of Medicine, Memorial Sloan Kettering Cancer Center, New York, New York 10065, USA. ²Lucille Castori Center for Microbes, Inflammation and Cancer, Memorial Sloan Kettering Cancer Center, New York, New York 10065, USA. ³Computational Biology Program, Sloan-Kettering Institute, New York, New York 10065, USA. ⁴Department of Biology, University of Massachusetts Dartmouth, North Dartmouth, Massachusetts 02747, USA. ⁵Donald B. and Catherine C. Marron Cancer Metabolism Center, Sloan-Kettering Institute, New York, New York 10065, USA. ⁶Genomics Core Laboratory, Sloan-Kettering Institute, New York, New York 10065, USA. ⁷Bone Marrow Transplant Service, Department of Medicine, Memorial Sloan Kettering Cancer Center, New York, New York 10065, USA. ⁸Immunology Program, Sloan-Kettering Institute, New York, New York 10065, USA.

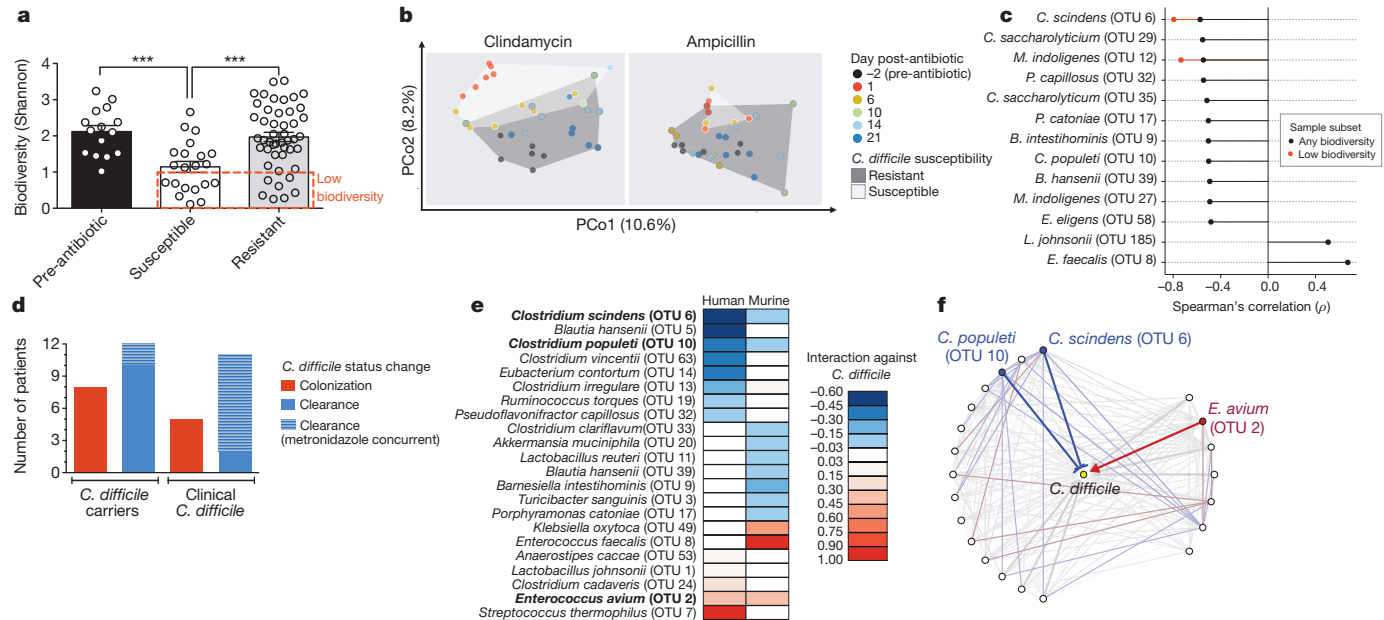


Figure 2 | Native intestinal bacterial species conserved across murine and human microbiota are predicted to inhibit *C. difficile* infection. Intestinal microbiota alpha diversity (a) and beta diversity (weighted UniFrac distances) (b) of antibiotic-naïve ($n = 15$) and antibiotic-exposed animals susceptible ($n = 21$) or resistant ($n = 47$) to *C. difficile* infection. c, Correlation of individual bacterial OTUs with susceptibility to *C. difficile* infection. d, Colonization (*C. difficile*-negative to -positive) and clearance (*C. difficile*-positive to -negative) events among *C. difficile*-diagnosed and carrier patients

low alpha diversity (Fig. 2a (red box)) or at early time points after antibiotic exposure (Fig. 2b), suggesting that recovery of more precise microbiota features (for example, individual species) contributed to infection resistance. We correlated resistance with individual bacterial species abundances, corresponding to operational taxonomic units (OTUs, $\geq 97\%$ 16S sequence similarity) (Extended Data Fig. 1d), and identified 11 bacterial OTUs that correlated strongly with infection resistance (Fig. 2c). These OTUs represented a small fraction of the microbiota membership (6%) and comprised primarily *Clostridium* cluster XIVa, including the OTU with the strongest resistance correlation, even among animals harbouring low alpha-diversity microbiota, *C. scindens* (Fig. 2c).

To relate intestinal bacterial species to *C. difficile* resistance in humans, we extended our study to a cohort of patients undergoing allogeneic haematopoietic stem-cell transplantation (allo-HSCT). The majority of these patients were diagnosed with a haematological malignancy and received chemotherapy and/or total body irradiation as well as antibiotics during transplantation (Extended Data Table 1), incurring reduced microbiota biodiversity associated with increased risk of bacterial blood stream infections⁸ and *C. difficile* infection⁹. Compared with controlled animal studies, temporal variation in antibiotic administration and sampling times among patients complicates analysis of relationships between microbiota composition and infection susceptibility. To address these challenges, we employed a recently developed systems biology approach¹⁰ that integrates antibiotic delivery schedules and time-resolved microbiota data to model mathematically the microbiota dynamics and infer which bacteria inhibit *C. difficile*. We included 24 allo-HSCT patients: 12 diagnosed with *C. difficile* infection and 12 who were *C. difficile* carriers without clinical infection (Fig. 2d and Extended Data Fig. 2). To facilitate comparisons across data sets, we clustered murine and human microbiota together to define OTUs that together accounted for a majority of both the human and mouse microbiota structure (Extended Data Fig. 3a–c), and applied the modelling approach to the murine study in parallel. We compared the normalized interaction networks from the human (Extended Data Fig. 3d) and the murine models

included in microbiota time-series inference modelling. Bacterial species with strong *C. difficile* interactions in human and murine microbiota models (e) that exist in a conserved subnetwork predicted to inhibit (blue) or positively associate (red) with *C. difficile* (f). Species interactions in bold type are common to mouse and human. *** $P < 0.001$. In c, $P < 0.0005$ ('any biodiversity', $n = 68$) or $P < 0.05$ ('Low biodiversity', Shannon diversity index ≤ 1 ($n = 16$ animals)). Centre values (mean), error bars (s.e.m.).

(Extended Data Fig. 3e) and identified bacteria displaying strong inhibition against *C. difficile*. Despite some differences across host species networks, the human model identified two *C. difficile*-inhibiting OTUs that were conserved in the murine model (Fig. 2e, f), the strongest of which was *C. scindens*, corroborating our murine correlation-based analyses (Fig. 2c).

To evaluate causality between intestinal bacteria identified in our analyses and infection resistance, we adoptively transferred resistance-associated bacteria. We cultured a representative consortium of four intestinal bacterial isolates with species-level 16S similarity to OTUs associated with *C. difficile* inhibition in our mouse and human analyses (Extended Data Fig. 4) and, after antibiotic administration, animals ($n = 10$) were administered a suspension containing the four-bacteria consortium or vehicle (phosphate-buffered saline (PBS)) before *C. difficile* infection. Additionally, since *C. scindens* had the strongest resistance associations in mice and humans (Fig. 2c, e), we included this bacterium in the consortium and in a third arm alone. Adoptive transfer of the consortium or *C. scindens* alone ameliorated *C. difficile* infection (Fig. 3a, b and Extended Data Fig. 5a) as well as associated weight loss (Fig. 3c and Extended Data Fig. 5b) and mortality (Fig. 3d) significantly compared with control. Transfer of the other three isolates individually, however, did not significantly enhance infection resistance (Extended Data Fig. 5c). Engraftment of the transferred bacteria was confirmed (Extended Data Fig. 5d) by 16S sequence comparison with the input and the native intestinal bacteria from our initial analyses (Fig. 2), thus fulfilling Koch's postulates (albeit for a microorganism and a beneficial health outcome). The abundance of *C. scindens* correlated significantly with infection resistance (Fig. 3e), suggesting that improving bacterial engraftment efficiency may enhance the protective effects of the adoptive transfer. Importantly, bacteria transfer was precise and engraftment did not alter other aspects of microbiota structure compared with control, including density (Extended Data Fig. 5e) and biodiversity (Fig. 3f).

We next interrogated the mechanism of *C. scindens*-mediated *C. difficile* inhibition. Some secondary bile acids can impair *C. difficile*

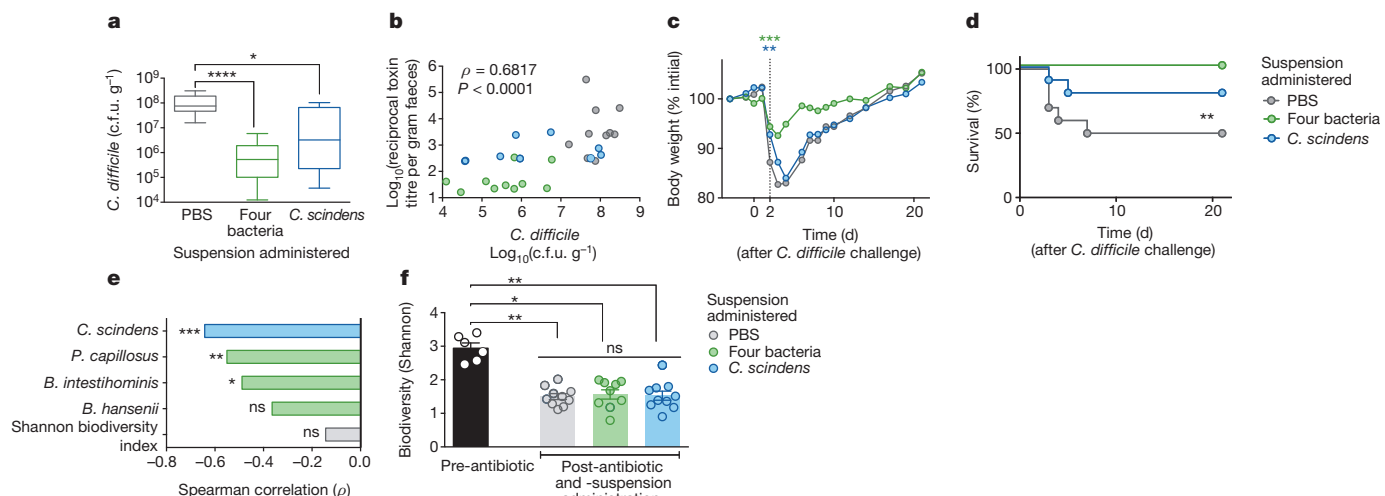


Figure 3 | Adoptive transfer of resistance-associated intestinal bacteria after antibiotic exposure increases resistance to *C. difficile* infection. Intestinal burden of *C. difficile* c.f.u. (a) and toxin (b) 24 h after *C. difficile* infection of antibiotic-exposed animals receiving adoptive transfers. Weight loss (c) and

growth *in vitro*^{11,12}, but the source and contribution of such metabolites to infection resistance *in vivo* remain unclear. Noting that *C. scindens* expresses enzymes crucial for secondary bile acid synthesis¹³ that are uncommon among intestinal bacteria¹⁴, we hypothesized that the *C. difficile*-protective effects of *C. scindens* may derive from this rare biosynthetic capacity. Analyses of antibiotic-exposed animals (Figs 1 and 2) revealed that recovery of secondary bile acids and the abundance of the gene family responsible for secondary bile acid biosynthesis (as predicted using PICRUSt¹⁵) correlated with *C. difficile* resistance (Fig. 4a,b). Targeted microbiome analysis of the gene family responsible for secondary bile acid biosynthesis indicated that abundance of the bile acid inducible (*bai*) operon genes correlated strongly with resistance to *C. difficile* infection (Fig. 4c) but that bile salt hydrolase (BSH)-encoding gene abundance did not. These results are consistent with reports indicating that BSH-encoding genes are distributed broadly while an extremely small fraction of intestinal bacteria possess a complete secondary bile acid synthesis pathway¹⁴. PCR-based assay of *baiCD*, which encodes

mortality (d) of animals after infection. e, Correlation of adoptively transferred bacteria engraftment (pre-infection) with *C. difficile* susceptibility. f, Microbiota biodiversity (pre-infection). ***P < 0.0001, **P < 0.01, *P < 0.05, NS (not significant). Mean (f); error bars, range (a), s.e.m. (f).

the 7 α -hydroxysteroid dehydrogenase enzyme critical for secondary bile acid biosynthesis, revealed that animals that had recovered *C. difficile* resistance after antibiotic exposure harboured a *baiCD*⁺ microbiome, whereas susceptible animals did not (Extended Data Fig. 6a).

Recipients of either the consortium or *C. scindens* harboured *baiCD*⁺ microbiomes with restored abundance of secondary bile acid biosynthesis genes (predicted by PICRUSt) (Extended Data Fig. 6b). Administration of either bacterial suspension also restored relative abundance of the secondary bile acids deoxycholate (DCA) (Fig. 4d) and lithocholate (LCA) (Extended Data Fig. 7a), both of which inhibit *C. difficile* in a dose-dependent fashion (Extended Data Fig. 8a,b), but abundances of primary bile acids were not significantly altered (Extended Data Fig. 7). Metagenomic inference indicated that consortium recipients harboured microbiomes with greater abundances of secondary bile acid biosynthesis genes than *C. scindens* recipients (Extended Data Fig. 6b), perhaps explaining their superior resistance to *C. difficile*. However, intestinal abundances of DCA and LCA were each comparable in the consortia

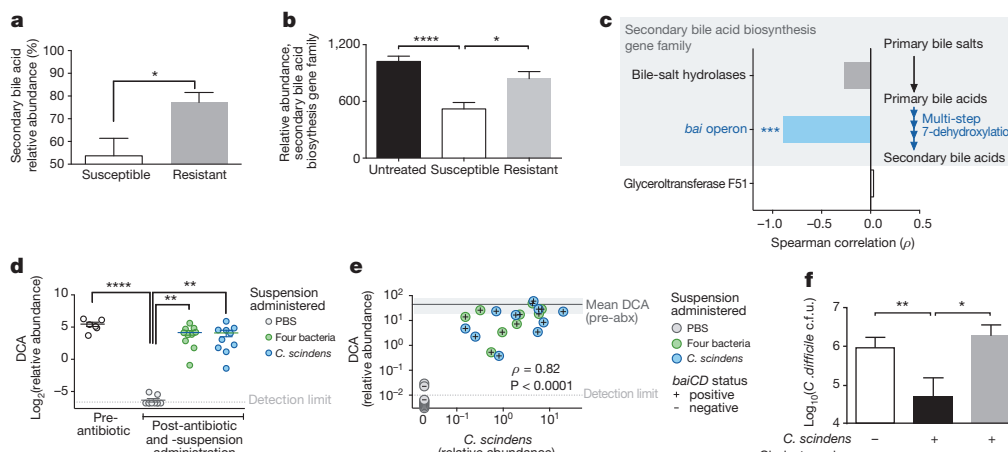


Figure 4 | *C. scindens*-mediated *C. difficile* inhibition is associated with secondary bile acid synthesis and is dependent on bile endogenous to intestinal content. Relative abundance of secondary bile acid species (a) and biosynthesis gene family abundance predicted by PICRUSt (b) in intestinal content from antibiotic-exposed *C. difficile* susceptible (n = 21), resistant (n = 47), and pre-antibiotic (n = 15) animals. c, Correlation of *C. difficile* susceptibility with the abundance of the gene family responsible for secondary bile acid biosynthesis in intestinal content (n = 6) quantified using shotgun

sequencing. d, Intestinal abundance of DCA after adoptive transfer of bacteria (n = 10 per group). e, Correlation of *C. scindens* engraftment with DCA abundance and *baiCD* status in intestinal content of antibiotic-exposed, adoptively transferred animals (n = 30). f, Bile acid dependent *C. scindens*-mediated inhibition of *C. difficile* quantified *ex vivo* (n = 6 per group). ***P < 0.0001, ***P < 0.001, **P < 0.01, *P < 0.05. Glyceroltransferase F51, endogenous reference gene (c). Shaded region around 'Mean DCA pre-abx' (pre-antibiotic), DCA abundance (s.d.) (e).

and *C. scindens* recipients pre-infection challenge (Fig. 4d and Extended Data Fig. 7a), suggesting additional mechanisms enhanced colonization resistance in consortia recipients. Indeed, of the four transferred bacteria, only *C. scindens* was *baiCD*⁺ (Extended Data Fig. 6a). Engraftment of *C. scindens* also correlated strongly with DCA relative abundance and *baiCD* in recipients, reaching levels observed in antibiotic-naïve animals (Fig. 4e), which indicated that precise transfer and efficient engraftment of this bacterium could restore physiological levels of secondary bile acid synthesis in antibiotic-exposed animals.

We evaluated bile acid dependent microbiota-mediated inhibition of *C. difficile* using an *ex vivo* model. Pre-incubation of intestinal content from antibiotic-naïve animals with cholestyramine, a bile acid sequestant¹⁶, permitted *C. difficile* growth (Extended Data Fig. 8c, d) comparable to intestinal content from antibiotic-exposed animals. Consistent with *in vivo* findings, introduction of *C. scindens* significantly inhibited *C. difficile* in the intestinal content from antibiotic-exposed animals. This effect was neutralized when intestinal content was pre-incubated with cholestyramine (Fig. 4f), indicating that *C. scindens*-mediated inhibition of *C. difficile* is dependent upon accessing and modifying endogenous bile salts and recapitulates a natural mechanism of microbiota-mediated infection resistance.

In summary, we show that a fraction of the intestinal microbiota as precise as a single bacterial species confers infection resistance by synthesizing *C. difficile*-inhibiting metabolites from host-derived bile salts. Our use of a human-derived *C. scindens* isolate to augment murine *C. difficile* inhibition emphasizes the conservation of this finding across species and suggests therapeutic and diagnostic applications. The genus *Clostridium* is phylogenetically complex^{17,18}, highlighting the value of integrating functional genomic and metabolomic interrogation with 16S rRNA profiling when evaluating probiotic candidates. Most bile-acid 7-dehydroxylating bacteria are cluster XIVa Clostridia closely related to one another^{14,19,20} and resistance-associated OTUs we identified, suggesting that *bai* or 16S gene signatures may serve as specific, functionally meaningful biomarkers for infection resistance. The replenishment of secondary bile acids and/or biosynthesis-competent bacteria (such as *C. scindens*) may contribute to the therapeutic efficacy of faecal microbiota transplant²¹. Attempts to manipulate intestinal bile acids directly should be performed with caution since some secondary bile acids have been linked to gastrointestinal cancers²². Other bacteria may augment resistance by enhancing 7-dehydroxylating Clostridia or through additional orthogonal mechanisms, such as competition for mucosal carbohydrates²³, activation of host immune defences^{24,25}, or production of antibacterial peptides²⁶. Knowledge of such mechanisms and the ecological context of those microbes responsible will facilitate amplification of microbiota-mediated pathogen resistance in individuals at risk of infection.

Online Content Methods, along with any additional Extended Data display items and Source Data, are available in the online version of the paper; references unique to these sections appear only in the online paper.

Received 4 May; accepted 3 September 2014.

Published online 22 October 2014; corrected online 7 January 2015 (see full-text HTML version for details).

- Buffie, C. G. & Pamer, E. G. Microbiota-mediated colonization resistance against intestinal pathogens. *Nature Rev. Immunol.* **13**, 790–801 (2013).
- Buffie, C. G. et al. Profound alterations of intestinal microbiota following a single dose of clindamycin results in sustained susceptibility to *Clostridium difficile*-induced colitis. *Infect. Immun.* **80**, 62–73 (2012).
- Rupnik, M., Wilcox, M. H. & Gerding, D. N. *Clostridium difficile* infection: new developments in epidemiology and pathogenesis. *Nature Rev. Microbiol.* **7**, 526–536 (2009).
- van Nood, E. et al. Duodenal infusion of donor feces for recurrent *Clostridium difficile*. *N. Engl. J. Med.* **368**, 407–415 (2013).
- Cimermancic, P. et al. Insights into secondary metabolism from a global analysis of prokaryotic biosynthetic gene clusters. *Cell* **158**, 412–421 (2014).

- Chang, J. Y. et al. Decreased diversity of the fecal microbiome in recurrent *Clostridium difficile*-associated diarrhea. *J. Infect. Dis.* **197**, 435–438 (2008).
- Lozupone, C. & Knight, R. UniFrac: a new phylogenetic method for comparing microbial communities. *Appl. Environ. Microbiol.* **71**, 8228–8235 (2005).
- Taur, Y. et al. Intestinal domination and the risk of bacteremia in patients undergoing allogeneic hematopoietic stem cell transplantation. *Clin. Infect. Dis.* **55**, 905–914 (2012).
- Kinnebrew, M. A. et al. Early *Clostridium difficile* infection during allogeneic hematopoietic stem cell transplantation. *PLoS ONE* **9**, e90158 (2014).
- Stein, R. R. et al. Ecological modeling from time-series inference: insight into dynamics and stability of intestinal microbiota. *PLOS Comput. Biol.* **9**, e1003388 (2013).
- Wilson, K. H. Efficiency of various bile salt preparations for stimulation of *Clostridium difficile* spore germination. *J. Clin. Microbiol.* **18**, 1017–1019 (1983).
- Sorg, J. A. & Sonenshein, A. L. Bile salts and glycine as cogerminants for *Clostridium difficile* spores. *J. Bacteriol.* **190**, 2505–2512 (2008).
- Kang, D. J., Ridlon, J. M., Moore, D. R., Barnes, S. & Hylemon, P. B. *Clostridium scindens* *baiCD* and *baiH* genes encode stereo-specific 7 α /7 β -hydroxy-3-oxo- Δ^4 -cholenic acid oxidoreductases. *Biochim. Biophys. Acta* **1781**, 16–25 (2008).
- Ridlon, J. M., Kang, D. J. & Hylemon, P. B. Bile salt biotransformations by human intestinal bacteria. *J. Lipid Res.* **47**, 241–259 (2006).
- Langille, M. G. et al. Predictive functional profiling of microbial communities using 16S rRNA marker gene sequences. *Nature Biotechnol.* **31**, 814–821 (2013).
- Out, C., Groen, A. K. & Brufau, G. Bile acid sequestrants: more than simple resins. *Curr. Opin. Lipidol.* **23**, 43–55 (2012).
- Collins, M. D. et al. The phylogeny of the genus *Clostridium*: proposal of five new genera and eleven new species combinations. *Int. J. Syst. Bacteriol.* **44**, 812–826 (1994).
- Yutin, N. & Galperin, M. Y. A genomic update on clostridial phylogeny: Gram-negative spore formers and other misplaced clostridia. *Environ. Microbiol.* **15**, 2631–2641 (2013).
- Kitahara, M., Takamine, F., Imamura, T. & Benno, Y. Assignment of *Eubacterium* sp. VPI 12708 and related strains with high bile acid 7 α -dehydroxylating activity to *Clostridium scindens* and proposal of *Clostridium hylemonae* sp. nov., isolated from human faeces. *Int. J. Syst. Evol. Microbiol.* **50**, 971–978 (2000).
- Wells, E. & Hylemon, B. Identification and characterization of a bile acid 7 α -dehydroxylating operon in *Clostridium* sp. strain TO-931, a highly active 7 α -dehydroxylating strain isolated from human feces. *Appl. Environ. Microbiol.* **66**, 1107–1113 (2000).
- Weingarden, A. R. et al. Microbiota transplantation restores normal fecal bile acid composition in recurrent *Clostridium difficile* infection. *Am. J. Physiol. Gastrointest. Liver Physiol.* **306**, G310–G319 (2014).
- Bernstein, H., Bernstein, C., Payne, C. M., Dvorakova, K. & Garewal, H. Bile acids as carcinogens in human gastrointestinal cancers. *Mutat. Res.* **589**, 47–65 (2005).
- Ng, K. M. et al. Microbiota-liberated host sugars facilitate post-antibiotic expansion of enteric pathogens. *Nature* **502**, 96–99 (2013).
- Jarchum, I., Liu, M., Shi, C., Equinda, M. & Pamer, E. G. Critical role for MyD88-mediated neutrophil recruitment during *Clostridium difficile* colitis. *Infect. Immun.* **80**, 2989–2996 (2012).
- Jarchum, I., Liu, M., Lipuma, L. & Pamer, E. G. Toll-like receptor 5 stimulation protects mice from acute *Clostridium difficile* colitis. *Infect. Immun.* **79**, 1498–1503 (2011).
- Rea, M. C. et al. Thuricin CD, a posttranslationally modified bacteriocin with a narrow spectrum of activity against *Clostridium difficile*. *Proc. Natl. Acad. Sci. USA* **107**, 9352–9357 (2010).

Acknowledgements E.G.P. received funding from US National Institutes of Health (NIH) grants R01 AI42135 and AI95706, and from the Tow Foundation. J.B.X. received funding from the NIH Office of the Director (DP2OD008440), NCI (U54 CA148967), and from a seed grant from the Lucile Castori Center for Microbes, Inflammation, and Cancer. C.G.B. was supported by a Medical Scientist Training Program grant from the National Institute of General Medical Sciences of the NIH (award number T32GM07739, awarded to the Weill Cornell/Rockefeller/Sloan-Kettering Tri-Institutional MD-PhD Program).

Author Contributions C.G.B. and E.G.P. designed the experiments and wrote the manuscript with input from co-authors. C.G.B. performed animal experiments and most analyses. V.B., R.R.S., J.B.X., C.S. and C.G.B. performed microbiota time-series inference modelling and analysis. P.T.M. and C.G.B. designed and performed *ex vivo* experiments. L.L., A.G., A.V. D.N. and M.K. performed 16S amplicon quantification and multiparallel sequencing (454, MiSeq) and contributed to data analysis. M.R.M.v.d.B., R.R.J., Y.T., E.L., C.G.B. and E.G.P. assessed clinical parameters and supervised patient cohort analysis. N.C.T. and C.G.B. performed metagenomic shotgun sequencing analysis. J.R.C. and H.L. developed the metabolomics analysis platform and performed quantification of bile acid species.

Author Information Study sequence data are deposited in the National Center for Biotechnology Information Sequence Read Archive under accession number SRP045811. Reprints and permissions information is available at www.nature.com/reprints. The authors declare no competing financial interests. Readers are welcome to comment on the online version of the paper. Correspondence and requests for materials should be addressed to E.G.P. (pamere@mskcc.org).

METHODS

Mouse husbandry. All experiments were performed with C57BL/6J female mice, 6–8 weeks old, purchased from Jackson Laboratories and housed in sterile cages with irradiated food and acidified water. Mouse handling and weekly cage changes were performed by investigators wearing sterile gowns, masks, and gloves in a sterile biosafety hood. All animals were maintained in a specific-pathogen-free facility at Memorial Sloan-Kettering Cancer Center Animal Resource Center. After co-housing for at least 2 weeks, animals (individuals or colonies, as indicated per experiment) were separately housed and randomly assigned to experimental groups. For experiments involving *C. difficile* infection, mice were administered 1,000 *C. difficile* VPI 10463 spores in PBS by oral gavage. All animal experiments were performed at least twice unless otherwise noted. Experiments were performed in compliance with Memorial Sloan-Kettering Cancer Center institutional guidelines and approved by the institution's Institutional Animal Care and Use Committee.

Murine *C. difficile* susceptibility time-course experiments. Mice from three separately housed colonies were kept in the same facility and administered clindamycin (administered by intraperitoneal injection, 200 µg daily), ampicillin (administered in drinking water, 0.1 g l⁻¹), or enrofloxacin (administered in drinking water, 0.4 g l⁻¹) for 3 days (days –2 to 0). At each time point after antibiotic cessation (days 1, 6, 10, 14, and 21), one mouse from each of the three colonies was randomly selected to be single-housed, infected with *C. difficile*, and analysed, yielding triplicate biological measurements per group, per time point. Intestinal content (faeces) was sampled before infection challenge for multiparallel 16S amplicon sequencing and microbiota structure analysis. *C. difficile* susceptibility was determined by selective culture and enumeration of c.f.u. from intestinal content (caecum and colon) 24 h after challenge.

Murine *in vivo* adoptive transfer experiments. Six colonies of mice ($n = 30$ total) were administered antibiotics as described previously²⁷ and subsequently individually housed and assigned randomly to one of three groups. Two days after antibiotics, groups of individually housed mice ($n = 10$ per group) received either 1,000,000 c.f.u. of a four-bacteria suspension (containing equal numbers of *C. scindens* (ATCC35704), *Barnesiella intestihominis* (isolated from murine faeces in-house), *Pseudoflavonifractor capillosus* (ATCC29799), and *Blautia hansenii* (ATCC27752)), a suspension containing 1,000,000 *C. scindens*, or vehicle (PBS) by gavage. All bacteria were grown under anaerobic conditions in reduced brain-heart infusion media supplemented with yeast extract and cysteine except for *B. intestihominis*, which was grown in liquid Wilkins–Chalgren media, and re-suspended in anaerobic PBS before administration to animals. Adoptive transfers of the suspensions were performed once daily for 2 consecutive days before challenge with *C. difficile* VPI 10463 (1,000 spores in PBS). *C. difficile* bacteria and cytotoxin were quantified in faecal samples obtained from mice 24 h after infection challenge. Animals were monitored for 21 days after infection challenge and weight loss was recorded.

Murine *ex vivo* adoptive transfer experiments. Three individually housed mice were administered 200 µg of clindamycin by intraperitoneal injection and killed 24 h later. Intestinal content was harvested from the ilea of killed animals, immediately transferred to an anaerobic chamber, and re-suspended in anaerobic PBS. Fractions containing 100 mg of intestinal content from each mouse were distributed and received either *C. scindens* (100,000 c.f.u.) or vehicle (anaerobic PBS). A third fraction was pre-treated with cholestyramine (1.5 mg) before receiving *C. scindens*. After transfer, the each suspension was inoculated with vegetative *C. difficile* (200 c.f.u.), incubated at 37 °C for 60 h, and *C. difficile* bacteria were quantified by overnight culture on selective media.

Quantitative *C. difficile* culture and toxin A and B. The quantities of *C. difficile* c.f.u. and cytotoxin in the intestinal (caecal) contents of animals were determined as described previously².

Enzymatic assay of secondary bile acid abundance. The relative abundances of primary and secondary bile acids in the intestinal content of killed animals was quantified using an enzymatic assay as described previously²⁸.

Sample collection and DNA extraction. Intestinal microbiota content samples were obtained, snap-frozen, stored, and DNA extracted as described previously²⁹. Briefly, a frozen aliquot (~100 mg) of each sample was suspended, while frozen, in a solution containing 500 µl of extraction buffer (200 mM Tris, pH 8.0/200 mM NaCl/20 mM EDTA), 200 µl of 20% SDS, 500 µl of phenol:chloroform:isoamyl alcohol (24:24:1), and 500 µl of 0.1-mm diameter zirconia/silica beads (BioSpec Products). Microbial cells were lysed by mechanical disruption with a bead beater (BioSpec Products) for 2 min, after which two rounds of phenol:chloroform:isoamyl alcohol extraction were performed. DNA was precipitated with ethanol and re-suspended in 50 µl of TE buffer with 100 µg ml⁻¹ RNase. The isolated DNA was subjected to additional purification with QIAamp Mini Spin Columns (Qiagen). Specimen collection from patients and analysis of the biospecimen group was approved by the Memorial Sloan-Kettering Cancer Center Institutional Review Board. All participants provided written consent for specimen collection and analysis.

Quantification 16S copy number density by rtPCR. DNA extracted from intestinal content samples (faeces) was subjected to rtPCR of 16S rRNA using 0.2 µM concentrations of the broad-range bacterial 16S primers 517F (5'-GCCAGCAG CCGCGTAA-3') and 798R (5'-AGGGTATCTAACCT-3') and the DyNAmo SYBR green rtPCR kit (Finnzymes). Standard curves were generated by serial dilution of the PCR blunt vector (Invitrogen) containing one copy of the 16S rRNA gene derived from a member of the Porphyromonadaceae family. The cycling conditions were as follows: 95 °C for 10 min, followed by 40 cycles of 95 °C for 30 s, 52 °C for 30 s, and 72 °C for 1 min.

Quantification of *baiCD* by PCR. DNA extracted from intestinal content samples (faeces) was subjected to PCR-based detection of the 7α-HSDH-encoding *baiCD* gene as described previously³⁰.

16S rRNA gene amplification and multiparallel sequencing. Amplicons of the V4–V5 16S rRNA region were amplified and sequenced using an Illumina MiSeq platform for samples in the *in vivo* and *ex vivo* adoptive transfer experiments. For each sample, duplicate 50-µl PCR reactions were performed, each containing 50 ng of purified DNA, 0.2 mM dNTPs, 1.5 mM MgCl₂, 1.25 U Platinum Taq DNA polymerase, 2.5 µl of 10× PCR buffer, and 0.2 µM of each primer designed to amplify the V4–V5: 563F (5'-nnnnnnnn-NNNNNNNNNNNN-AYTGGGYDTAAAGN G-3') and 926R (5'- nnnnnnnn-NNNNNNNNNNNN-CCGTCAATTYHTTR AGT-3'). A unique 12-base Golay barcode (Ns) preceded the primers for sample identification³¹, and one to eight additional nucleotides were placed in front of the barcode to offset the sequencing of the primers. Cycling conditions were 94 °C for 3 min, followed by 27 cycles of 94 °C for 50 s, 51 °C for 30 s, and 72 °C for 1 min. A condition of 72 °C for 5 min was used for the final elongation step. Replicate PCRs were pooled, and amplicons were purified using the Qiaquick PCR Purification Kit (Qiagen). PCR products were quantified and pooled at equimolar amounts before Illumina barcodes and adaptors were ligated on using the Illumina TruSeq Sample Preparation protocol. The completed library was sequenced on an Illumina MiSeq platform following the Illumina recommended procedures. Samples in the murine and human *C. difficile* susceptibility time-course experiments were sequenced using the 454 FLX Titanium platform as described previously³². Sequences from allo-HSCT patients were obtained from a previously published study⁸.

Sequence analysis. Sequences were analysed using the mothur³³ (version 1.33.3) pipeline. Potentially chimaeric sequences were removed using the UChime algorithm³⁴. Sequences with a distance-based similarity of 97% or greater were grouped into OTUs using the average neighbour algorithm and classified using the BLAST (megablast) algorithm and the GenBank 16S rRNA reference database; OTU-based microbial diversity was estimated by calculating the Shannon diversity index. Sequence abundance profiles in each sample were used for downstream statistical and modelling analysis. A phylogenetic tree was inferred using Clearcut³⁵, on the 16S rRNA sequence alignment generated by mothur; unweighted UniFrac⁷ was run using the resulting tree, and principal coordinate analysis was performed on the resulting matrix of distances between each pair of samples. PICRUSt (version 0.9.1)¹⁵ in combination with QIIME (version 1.6.0)³⁶ was used to predict abundances of the gene family responsible for secondary bile acid biosynthesis (KEGG pathway ko00121) for a set of 83 samples. Maximum likelihood phylogenetic trees (Kimura model, bootstrap of 100 replicates) were constructed using the MEGA 6.06 package from representative sequences of intestinal bacteria as described³⁷. Raw sequence data from metagenomic shotgun sequencing of six intestinal (ileal) microbiome samples were pre-processed to remove mouse-derived, duplicate, and low-quality reads as well as low-quality bases in accordance with Human Microbiome Project protocols³⁸. The remaining reads were mapped against a set of proteins associated with the secondary bile acid biosynthesis pathway using RAPSearch version 2.07 (ref. 39). For the subsequent analysis, only hits with an *E* value ≤ 0.1 , a minimum alignment length of 30, and a minimum similarity of 50% were considered.

Quantification of secondary bile acid species. Samples of murine intestinal content (faeces, ~30 mg) were homogenized using a handheld homogenizer (Omni International) in 80% aqueous methanol and corrected to a final concentration of 0.5 mg per 10 µl. Samples were then sonicated using a Diagenode sonicator at high power, 6 × 30 s cycles. Four hundred microlitres of this material were removed and 20 µl of internal standard added (25 µM d4-chenodeoxycholic acid in 55%/45% methanol/water (v/v)). A further 1 ml methanol was added to the extract and samples were vortexed at 1,400 r.p.m. for 1 h at 30 °C (Thermomixer, Eppendorf). Remaining solid material was removed by centrifugation (21,000g for 10 min) and the supernatant transferred to a glass tube. A second extraction was performed using 1.5 ml methanol, and combined supernatants were dried under a nitrogen gas stream. Finally samples were re-suspended in 300 µl 55%/45% methanol/water (v/v), filtered through a 3 kDa molecular weight cut-off cartridge (Millipore), and transferred to a mass spectrometry vial containing a reduced volume glass insert. Bile acids were separated using an Agilent 1290 HPLC and Cogent C18 column (2.1 mm × 150 mm, 2.2 µm; MicroSolv Technology). Mobile phase A: water + 0.05% formic acid; mobile phase B: acetone + 0.05% formic acid; flow rate 0.35 ml min⁻¹. Injection volume was

5 µl and the liquid chromatography gradient was from 25% B to 70% B in 25 min. Bile acids were detected using an Agilent 6550 Q-TOF mass spectrometer with JetStream source, operating in negative ionization mode and extended dynamic range. Acquisition was from *m/z*: 50–1,100 at one spectrum per second; gas temperature: 275 °C; drying gas: 11 l min⁻¹; nebulizer: 30 psig; sheath gas: 325 °C; sheath gas flow 10 l min⁻¹; *V*_{Cap} 4000 V; fragmentor 365 V and Oct 1 RF 750 V. Bile acids (Extended Data Table 2) were identified by their exact mass and confirmed by chromatographic alignment to authentic standards (purchased from Steraloids or Sigma Aldrich). Abundances of the M-H and M+formate ions were then extracted and summed using ProFinder software (Agilent Technologies) and normalized to the internal standard abundance using Mass Profiler Professional software (Agilent Technologies).

DCA and LCA. *C. difficile* inhibition assays. Growth of *C. difficile* in brain–heart infusion liquid media supplemented with yeast extract and cysteine, with added DCA (0.1%, 0.01%, 0.001%, final concentration, in water vehicle) or LCA (0.01%, 0.001%, final concentration, in 100% ethanol vehicle), or vehicle alone was monitored by attenuation (*D*_{600 nm}) using a spectrophotometer.

Statistics. Statistical analyses were performed using the R (v. 3.0.2) and GraphPad Prism (version 6.0c) software packages. The Mann–Whitney rank sum test (two-tailed) was used for comparisons of continuous variables between two groups with similar variances; the Kruskal–Wallis test with Dunn correction for multiple comparisons was used for comparisons of three groups or more (*n* ≥ 5 samples per group) with similar variances. In all experiments involving group comparisons, at least six animals were used per group; for these non-parametric tests, it was calculated that a sample size of six per group would be sufficient to detect an effect size of 2 with 90% power ($\alpha = 0.05$)⁴⁰. Data were visualized using bar plots with centre values representing the mean and error bars representing standard error of the mean, and box plots representing the median and interquartile range of the upper and lower quartiles and error bars showing the range. Spearman rank correlation tests (two-tailed) were used to find significant correlations between two continuous variables. After statistical analyses with multiple comparisons, we used the Benjamini–Hochberg method to control the false discovery rate. The log-rank test was used to find significant differences in the survival distributions among *C. difficile*-challenged groups of animals. When possible, investigators were blinded during group allocation and outcome assessment (16S and metagenomic shotgun sequence collection, extraction, quantification, and analysis; microbiota time-series inference modelling; quantification of bile species by enzymatic assay and high-performance liquid chromatography–mass spectrometry; enumeration of *C. difficile* in animal experiments).

Inference modelling of mouse microbiota time-series. To determine the network of bacterial–bacterial interactions and extract native resident bacteria with *C. difficile* inhibitory properties, we applied the Lotka–Volterra dynamics-based framework of ref. 10 to the mouse data set. This inference framework consists of a regularized least-square regression of the observed data points and the known antibiotic signal against the difference of the log-transformed total abundances in time:

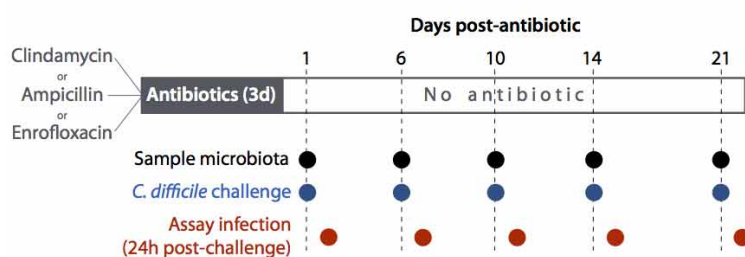
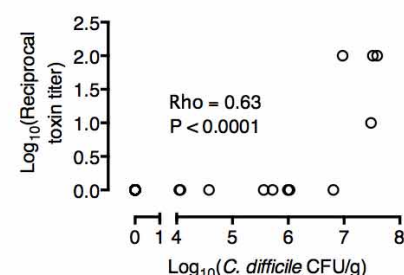
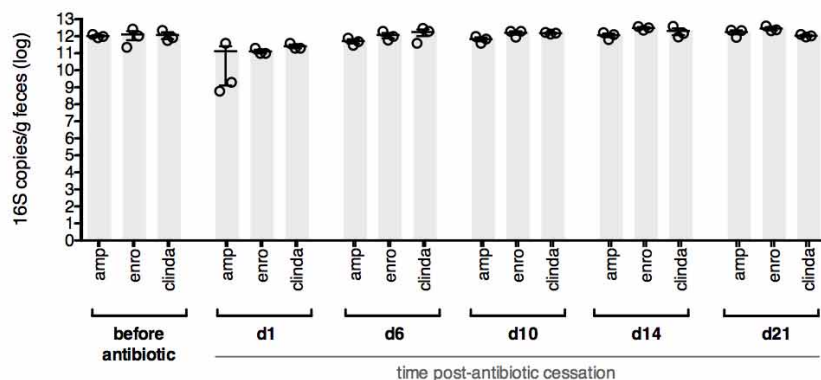
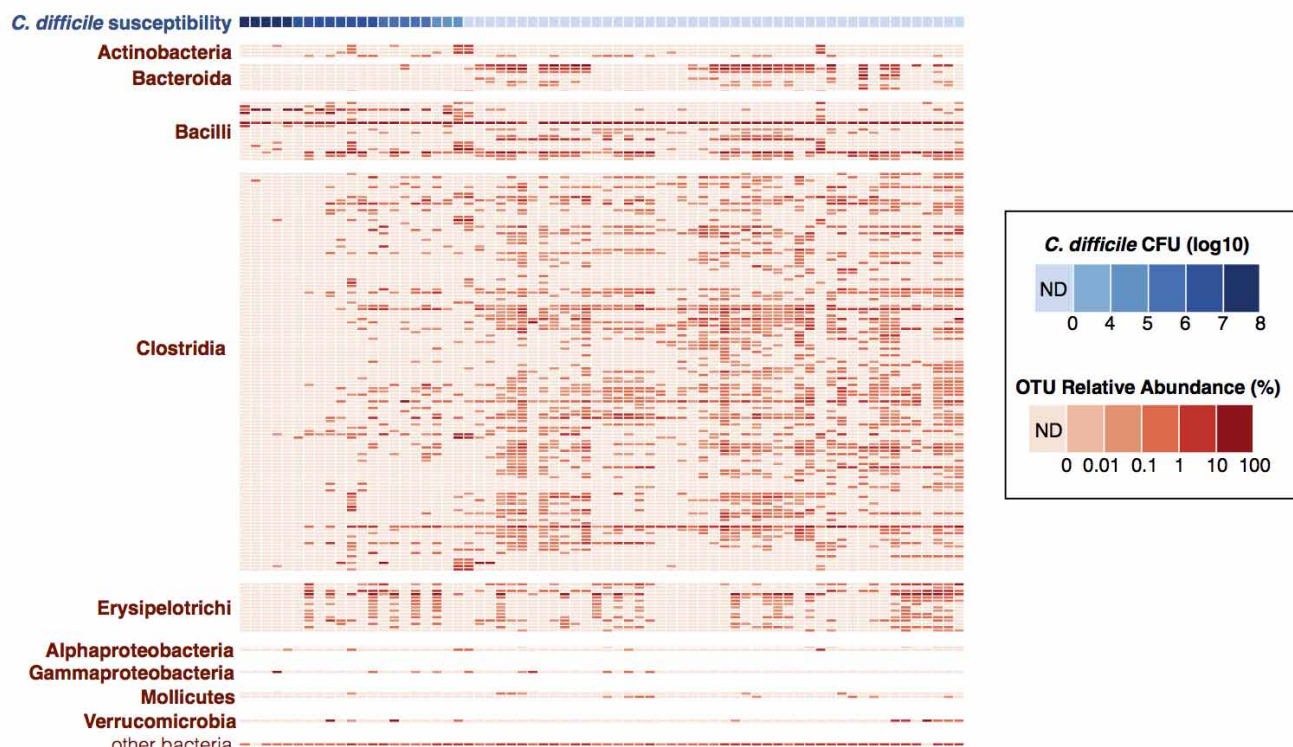
$$\frac{\Delta \ln x_i(t)}{\Delta t} = [\ln(x_i(t + \Delta t)) - \ln(x_i(t))] / \Delta t$$

with *i* = 1 … *N*, where *N* is the total number of considered OTUs. This results in coefficients characterizing growth, directed interactions, and susceptibilities of each OTU to the external perturbations. The method requires temporal profiles of total abundances of each of the 36 representative OTUs, which were obtained by scaling their normalized abundance from the pyrosequencing run (fraction ranging from 0 to 1) by the total amount of bacteria DNA recovered from each gram of stool or intestinal content. The temporal profile of the *C. difficile* total abundance was obtained from the c.f.u. counts recovered by plating the caecal content after

mouse euthanasia. The last time differences, $\Delta \ln x_i(t_{\text{inoc}})$, were calculated for each mouse as the difference between the total abundance in the intestinal content (faeces) on the day after *C. difficile* inoculation, *t*_{inoc}, (also the day of mouse euthanasia) minus the total abundance in the content (faeces) before *C. difficile* infection or $\Delta \ln x_i(t_{\text{inoc}}) = \ln x_i^{\text{colon}}(t_{\text{inoc}} + 1) - \ln x_i^{\text{faeces}}(t_{\text{inoc}})$. Similarly the differential profile for *C. difficile* was evaluated from the log-difference in the scaled colony counts for the corresponding faecal and caecal samples. Antibiotic perturbations (ampicillin, clindamycin, or enrofloxacin) were modelled as a discrete signal when administered at day –2 (Fig. 1). The inference algorithm was run on a total of 240 samples and the global model was selected with a threefold cross-validation scheme on the 75 combined time courses to ensure robustness to the introduction of unseen data¹⁰. In particular, the number of data points outnumbers the number of unknowns; that is, the linear system to be solved is overdetermined, ensuring a sufficient number of constraints by the data for inferring the unknown coefficients.

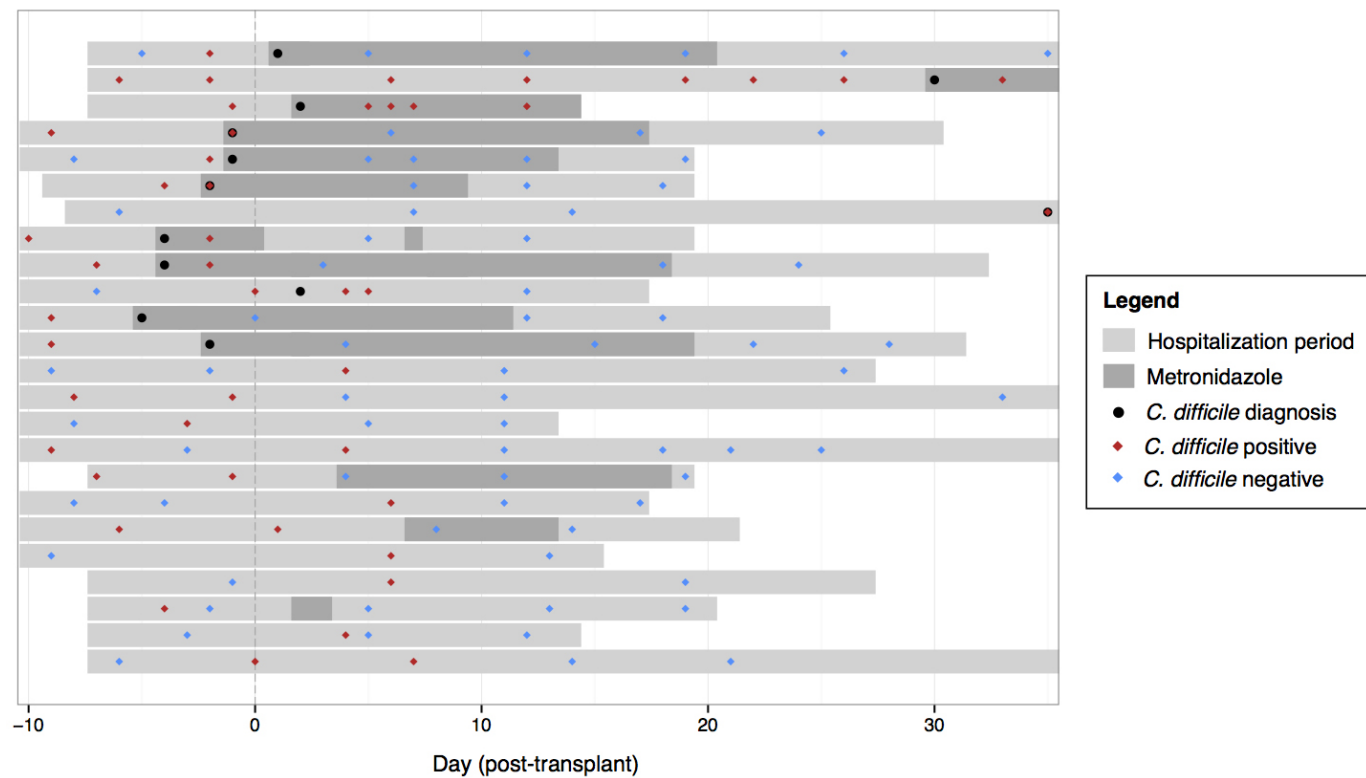
Inference modelling of allo-HSCT patient microbiota time-series. To determine whether commensal–*C. difficile* interactions observed in the mouse data were also conserved in humans, we applied the same inference-modelling framework to data from 24 allo-HSCT hospitalized patients. As above, for each of the 36 OTUs, we determined the log-differential in total abundance as the log-difference of the normalized abundance scaled by the corresponding total bacterial DNA per gram of stool at the next sampling event minus the total abundance at the current sampling time. Differential abundance in *C. difficile* was determined from the rtPCR measurements of the *C. difficile* 16S rRNA gene per gram of faeces. Similarly to the above, we ran the algorithm on a total of 112 samples and the global model was selected applying a threefold cross-validation scheme on the 24 combined time courses. This choice again yields an overdetermined linear system to be solved.

27. Chen, X. *et al.* A mouse model of *Clostridium difficile*-associated disease. *Gastroenterology* **135**, 1984–1992 (2008).
28. Giel, J. L., Sorg, J. A., Sonenshein, A. L. & Zhu, J. Metabolism of bile salts in mice influences spore germination in *Clostridium difficile*. *PLoS ONE* **5**, e8740 (2010).
29. Ubeda, C. *et al.* Vancomycin-resistant *Enterococcus* domination of intestinal microbiota is enabled by antibiotic treatment in mice and precedes bloodstream invasion in humans. *J. Clin. Invest.* **120**, 4332–4341 (2010).
30. Wells, J. E., Williams, K. B., Whitehead, T. R., Heuman, D. M. & Hylemon, P. B. Development and application of a polymerase chain reaction assay for the detection and enumeration of bile acid 7α-dehydroxylating bacteria in human feces. *Clin. Chim. Acta* **331**, 127–134 (2003).
31. Caporaso, J. G. *et al.* Ultra-high-throughput microbial community analysis on the Illumina HiSeq and MiSeq platforms. *ISME J.* **6**, 1621–1624 (2012).
32. Ubeda, C. *et al.* Intestinal microbiota containing *Barnesiella* cures vancomycin-resistant *Enterococcus faecium* colonization. *Infect. Immun.* **81**, 965–973 (2013).
33. Schloss, P. D. *et al.* Introducing mothur: open-source, platform-independent, community-supported software for describing and comparing microbial communities. *Appl. Environ. Microbiol.* **75**, 7537–7541 (2009).
34. Edgar, R. C., Haas, B. J., Clemente, J. C., Quince, C. & Knight, R. UCHIME improves sensitivity and speed of chimera detection. *Bioinformatics* **27**, 2194–2200 (2011).
35. Sheneman, L., Evans, J. & Foster, J. A. Clearcut: a fast implementation of relaxed neighbor joining. *Bioinformatics* **22**, 2823–2824 (2006).
36. Caporaso, J. G. *et al.* QIIME allows analysis of high-throughput community sequencing data. *Nature Methods* **7**, 335–336 (2010).
37. Hall, B. G. Building phylogenetic trees from molecular data with MEGA. *Mol. Biol. Evol.* **30**, 1229–1235 (2013).
38. Human Microbiome Project Consortium Structure. Function and diversity of the healthy human microbiome. *Nature* **486**, 207–214 (2012).
39. Zhao, Y., Tang, H. & Ye, Y. RAPSearch2: a fast and memory-efficient protein similarity search tool for next-generation sequencing data. *Bioinformatics* **28**, 125–126 (2012).
40. Cohen, J. *Statistical Power Analysis for the Behavioral Sciences* (Routledge, 1988).

a**b****c****d**

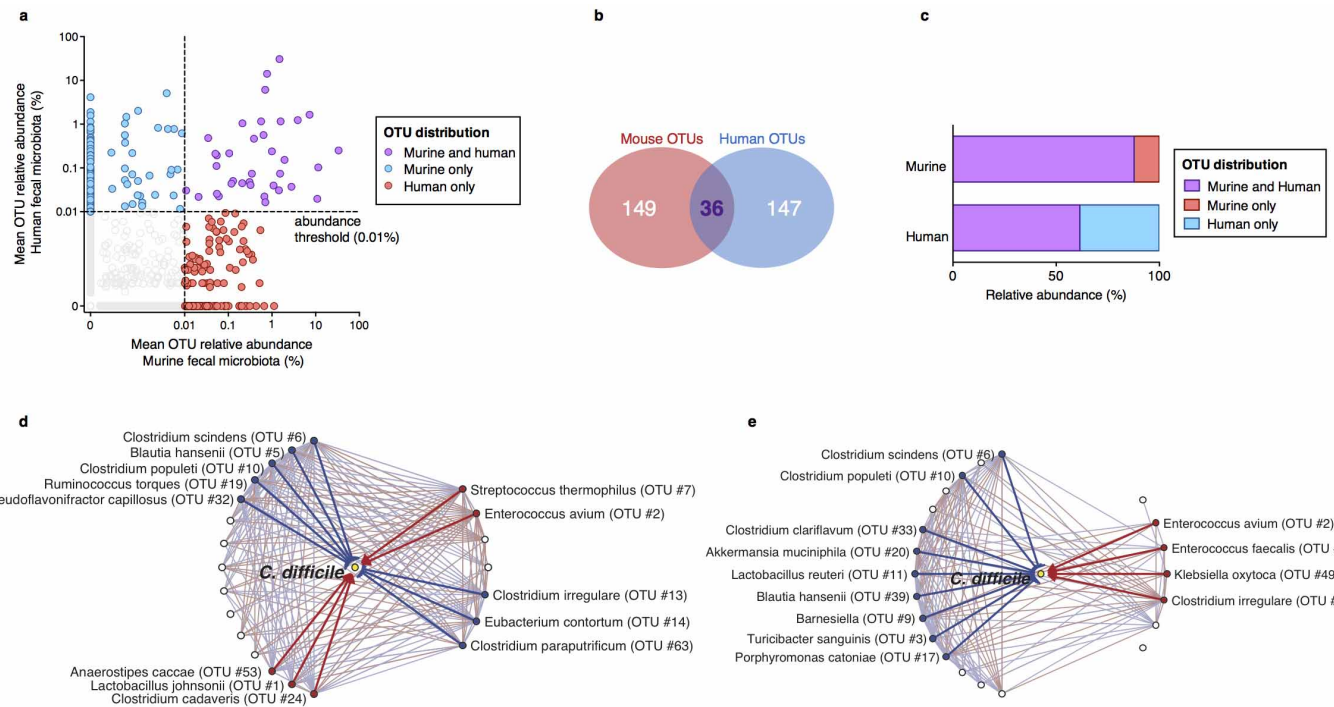
Extended Data Figure 1 | Dynamics of intestinal microbiota structure and *C. difficile* susceptibility after antibiotic exposure. **a**, Strategy for determining *C. difficile* susceptibility duration post-antibiotic exposure ($n=3$ separately-housed mouse colonies per antibiotic arm) and relating infection resistance to microbiota structure. **b**, Correlation of *C. difficile* c.f.u. and toxin in intestinal content following infection. **c**, Intestinal bacterial density of animals

before and after antibiotic exposure. **d**, Relative abundance of bacterial OTUs ($\geq 97\%$ sequence similarity, $>0.01\%$ relative abundance) sorted by class (red) and corresponding *C. difficile* susceptibility (blue) among antibiotic-exposed mice ($n=68$) allowed to recover for variable time intervals prior to *C. difficile* infection challenge. Centre values (mean), error bars (s.e.m.) (c). ND, not detectable.



Extended Data Figure 2 | Allo-HSCT patient timelines and *C. difficile* infection status transitions. Transitions between *C. difficile* (*tcDB*-positive) colonization status in patients receiving allogeneic haematopoietic stem-cell transplantation, as measured by *C. difficile* 16S rRNA abundance during the period of hospitalization (light grey bars). Time points when *C. difficile*

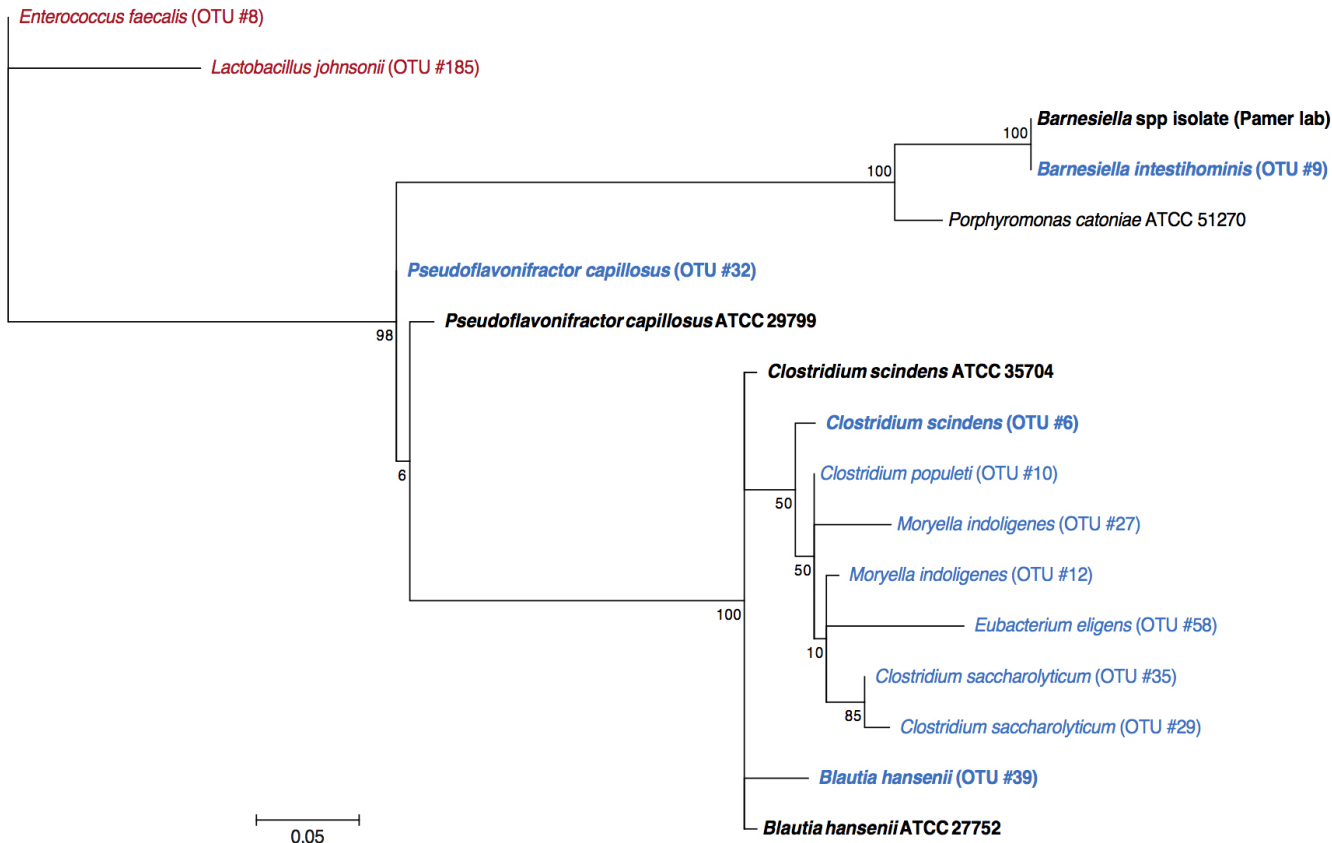
colonization was determined to be positive (red diamonds) and negative (blue diamonds), and when *C. difficile* infection was clinically diagnosed (black dots) and metronidazole was administered (dark grey bars), are displayed relative to the time of transplantation per patient.



Extended Data Figure 3 | Identification of bacteria conserved across human and murine intestinal microbiota predicted to inhibit *C. difficile*.

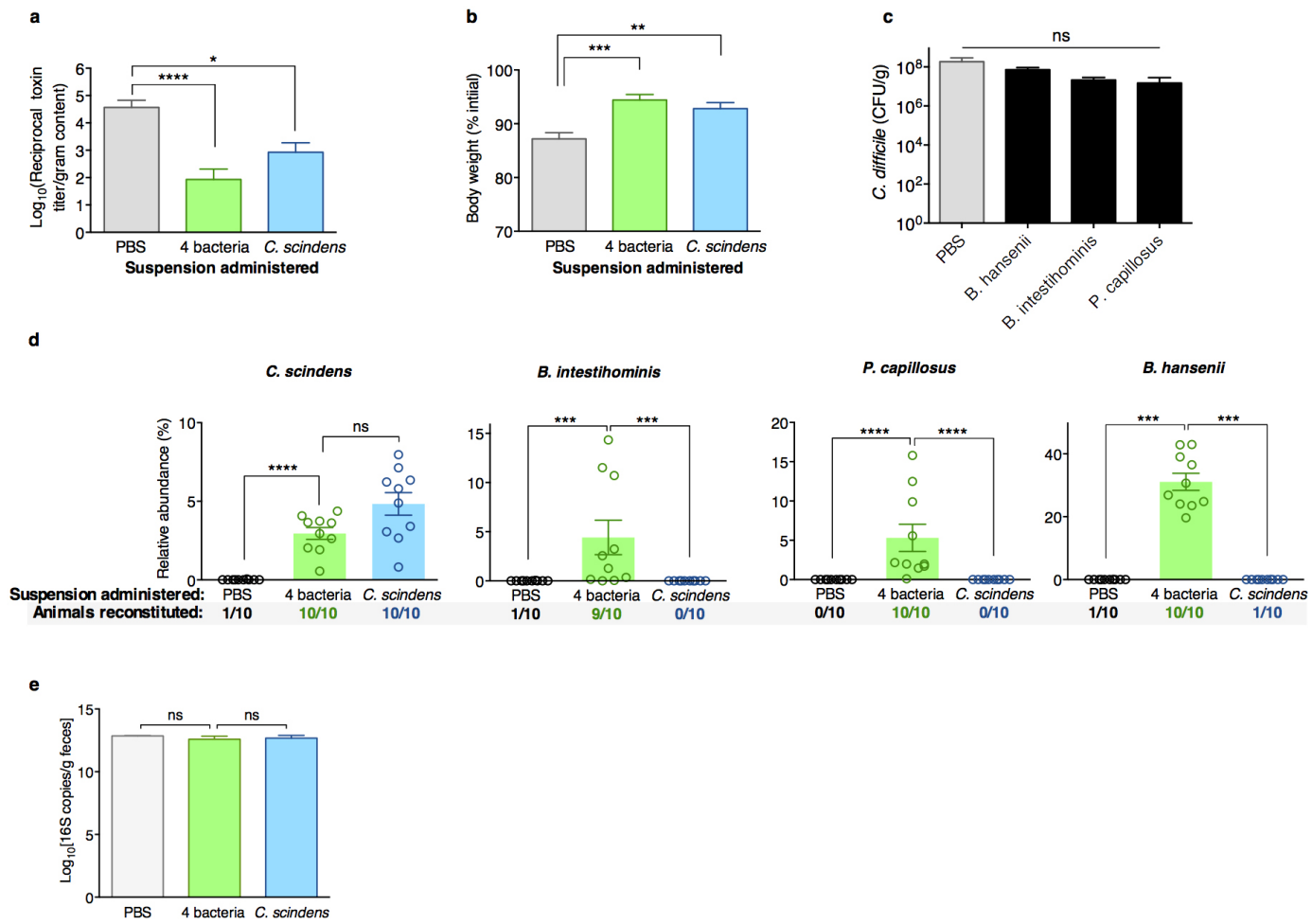
Identification of bacterial OTUs abundant in mice ($n = 68$) and humans ($n = 24$) (a) that account for a minority of OTU membership (b) but the

majority of the structure of the intestinal microbiota of both host species after antibiotic exposure (c). Subnetworks of abundant OTUs predicted inhibit (blue) or positively associate with (red) *C. difficile* in murine (d) and human (e) intestinal microbiota.



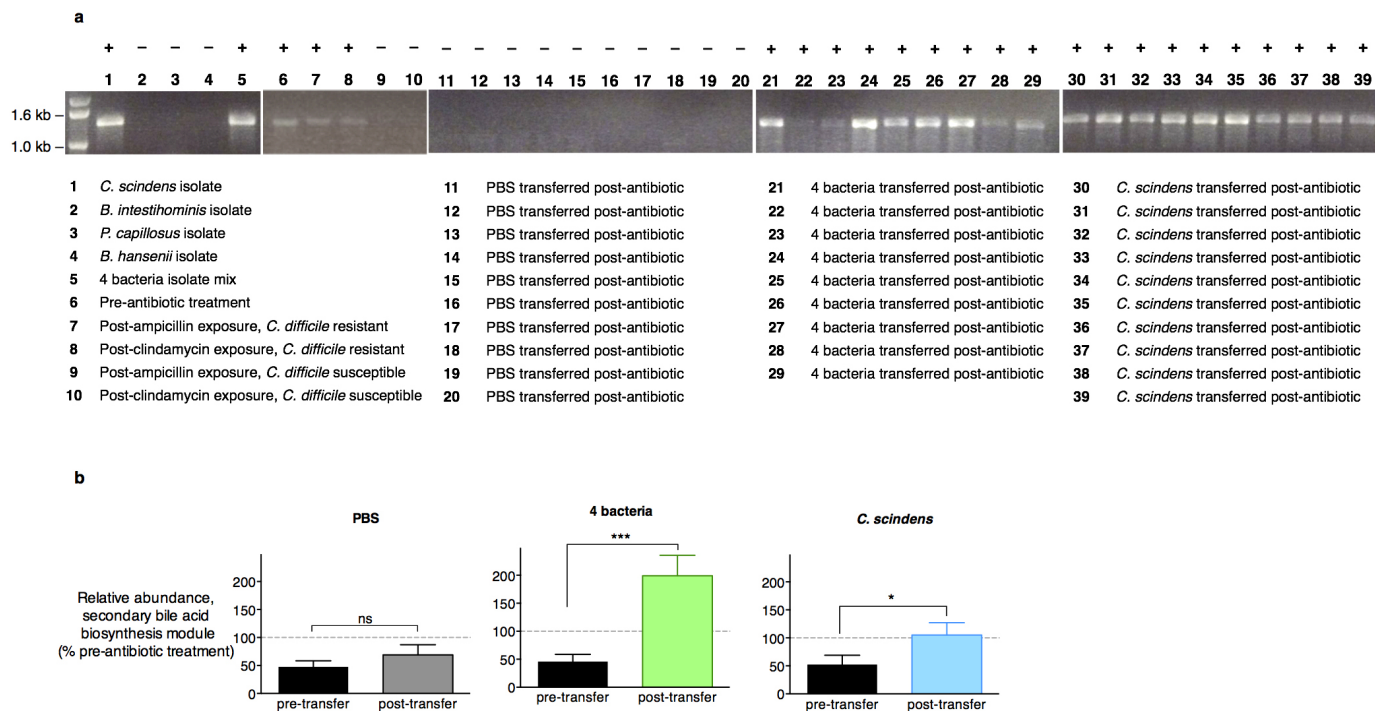
Extended Data Figure 4 | Phylogenetic distribution of resistance-associated intestinal bacteria and isolates selected for adoptive transfer. The maximum likelihood phylogenetic tree (Kimura model, bootstrap of 100 replicates) was constructed using the MEGA 6.06 package from representative sequences of

intestinal bacteria associated with resistance to *C. difficile* infection (blue), including cultured representatives subsequently used in adoptive transfer experiments (**bold**). The tree was rooted using intestinal bacteria associated with susceptibility to infection (red) as an outgroup.



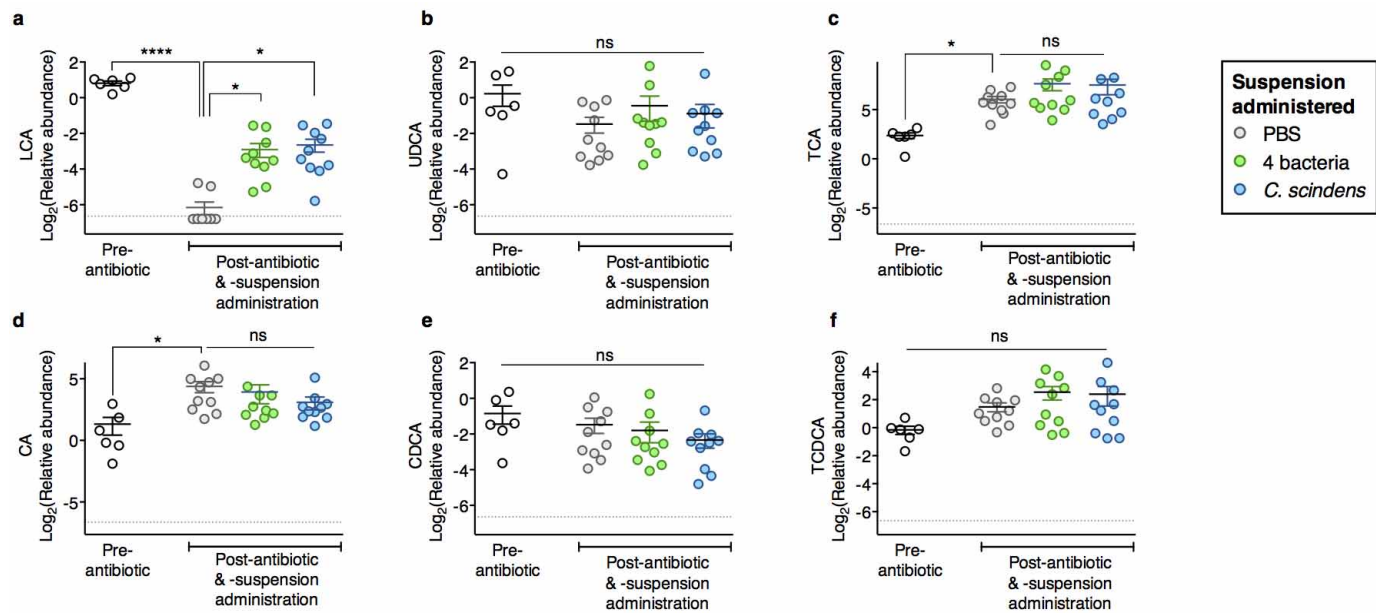
Extended Data Figure 5 | Adoptive transfer and engraftment of four-bacteria consortium or *C. scindens* ameliorates intestinal *C. difficile* cytotoxin load and acute *C. difficile*-associated weight loss. **a**, *C. difficile* toxin load in antibiotic-exposed animals receiving adoptive transfers 24 h after *C. difficile* infection challenge. Animals' weights 48 h after infection challenge and **(b)** *C. difficile* c.f.u. 24 h after infection challenge **(c)**. **d**, Engraftment of bacterial isolates in the intestinal microbiota of antibiotic-exposed animals 2 days after adoptive transfer of *B. intestihominis*, *P. capillosus*, *B. hansenii*, and/or *C. scindens*. **e**, Intestinal bacterial density (faeces) from antibiotic-exposed

mice administered suspensions containing four bacteria, *C. scindens*, or vehicle (PBS) as measured by rtPCR of 16S rRNA genes. ***P < 0.0001, ***P < 0.001, **P < 0.01, *P < 0.05; Mann–Whitney (two-tailed) (a, b, d, e), Kruskal–Wallis with Dunn correction (c) (n = 6–10 per group). Centre values, mean; error bars, s.e.m. Results are representative of at least two independent experiments. Numbers under group columns in **d** denote the number of mice with detectable engraftment of the given bacterium (out of ten possible separately housed animals per group).



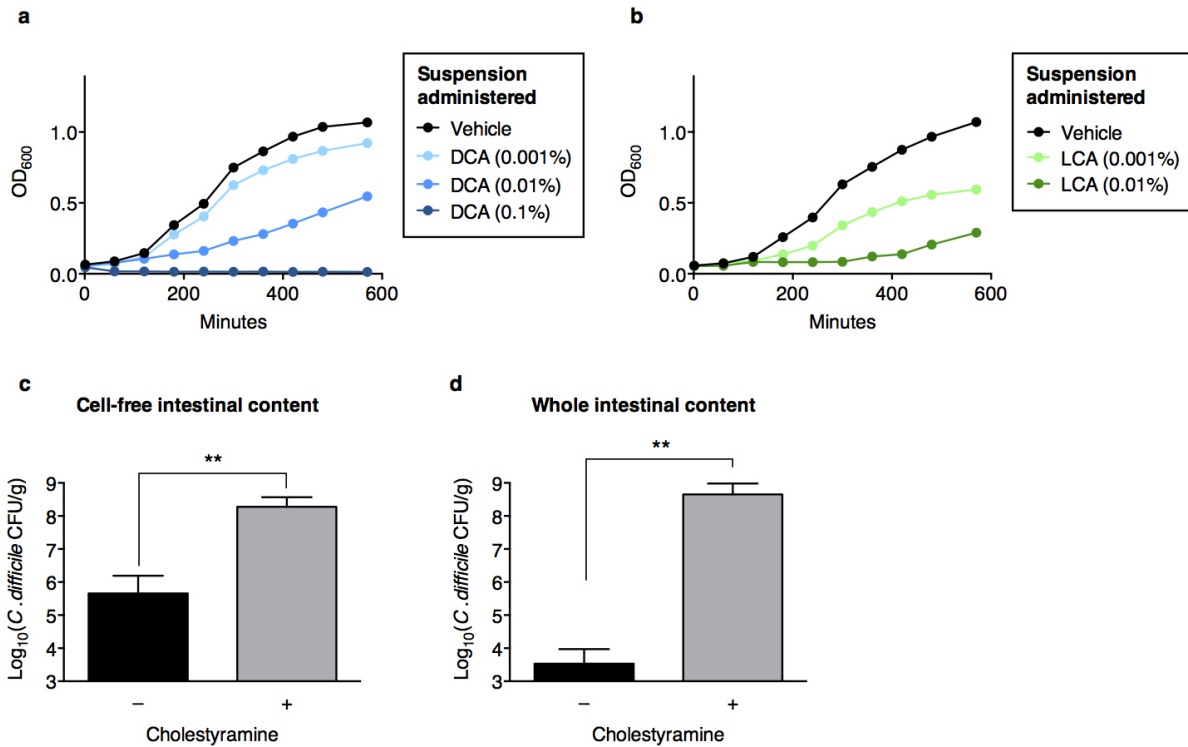
Extended Data Figure 6 | Adoptive transfer of consortia or *C. scindens* restores *baiCD* and the abundance of the gene family responsible for secondary bile acid biosynthesis. **a**, PCR-based detection of the 7 α -HSDH-encoding *baiCD* gene in bacterial isolates, intestinal microbiomes (faeces) of animals before antibiotic exposure, and intestinal microbiomes (faeces) of animals that, after antibiotic exposure, remained susceptible to *C. difficile* or

recovered resistance to infection spontaneously or after adoptive transfer of bacterial isolates. **b**, Reconstituted abundance of the gene family responsible for secondary bile acid biosynthesis, as predicted by PICRUSt, in antibiotic-exposed animals receiving adoptive transfers ($n = 10$ per group). *** $P < 0.001$; * $P < 0.05$; NS, not significant; Mann–Whitney (two-tailed) (**b**). Centre values, mean; error bars, s.e.m.



Extended Data Figure 7 | Impacts of adoptive transfers of bacteria on intestinal abundance of bile acids. Intestinal abundance of the secondary bile acids LCA (a), ursodeoxycholate (UDCA) (b), and primary bile acids (c–f) in

mice after antibiotic exposure and adoptive transfer of bacteria indicated. ***P < 0.0001, *P < 0.05, NS (not significant); Kruskal–Wallis test with Dunn’s correction. Centre values, mean; error bars, s.e.m.



Extended Data Figure 8 | *C. difficile* growth inhibition by secondary bile acids and intestinal content from antibiotic-naive animals. Addition of the secondary bile acids DCA (a) or LCA (b) to culture media inhibits *C. difficile*. Bile acid dependent inhibition of *C. difficile* enumerated by recovery of c.f.u.

after inoculation of vegetative *C. difficile* into cell-free (c) or whole (d) intestinal content harvested from C57BL/6J mice ($n = 5$ or 6 per group), with or without pre-incubation with cholestyramine. ** $P < 0.01$; Mann–Whitney (two-tailed) (c, d).

Extended Data Table 1 | Characteristics of patients and transplant course

Parameter	No. (% of patients)
Age (years)	
≤29	2/24 (8.3%)
30-39	5/24 (20.8%)
40-49	2/24 (8.3%)
50-59	6/24 (25.0%)
≥60	9/24 (37.5%)
Sex (female)	10/24 (41.7%)
Underlying Disease	
Leukemia	11/24 (45.8%)
Lymphoma	5/24 (20.8%)
Multiple Myeloma	3/24 (12.5%)
Myelodysplastic Syndrome	3/24 (12.5%)
Other	2/24 (8.3%)
Conditioning Intensity	
Nonmyeloablative	4/24 (16.7%)
Reduced intensity	4/24 (16.7%)
Myeloablative	16/24 (66.7%)
T-cell depletion	13/24 (54.2%)
Stem cell source (cord vs. other)	5/24 (20.8%)
Time to engraftment (≥ 14 d) ^{*†}	5/24 (20.8%)
Fever ($T \geq 100.4$) [†]	21/24 (87.5%)
Vital Status: Dead [†]	1/24 (4.2%)
Total	24/24 (100.0%)

* Engraftment was defined as an absolute neutrophil count of more than 500 cells per microlitre for 3 consecutive days.

† Assessed during inpatient allogeneic haematopoietic stem-cell transplantation hospitalization (from 15 days before transplant to 35 days after transplant).

Extended Data Table 2 | Retention times for bile acids quantified by high-performance liquid chromatography–mass spectrometry

Compound	Molecular formula	Accurate mass	Retention time (min)	CAS number
LCA	C ₂₄ H ₄₀ O ₃	376.29775	24.16	434-13-9
UDCA	C ₂₄ H ₄₀ O ₄	392.29266	16.59	128-13-2
DCA	C ₂₄ H ₄₀ O ₄	392.29266	20.42	83-44-3